

# We are IntechOpen, the world's leading publisher of Open Access books Built by scientists, for scientists

6,900

Open access books available

186,000

International authors and editors

200M

Downloads

Our authors are among the

154

Countries delivered to

TOP 1%

most cited scientists

12.2%

Contributors from top 500 universities



WEB OF SCIENCE™

Selection of our books indexed in the Book Citation Index  
in Web of Science™ Core Collection (BKCI)

Interested in publishing with us?  
Contact [book.department@intechopen.com](mailto:book.department@intechopen.com)

Numbers displayed above are based on latest data collected.  
For more information visit [www.intechopen.com](http://www.intechopen.com)



---

# Active and Reactive Power Control of Wound Rotor Induction Generators by Using the Computer and Driver

---

Fevzi Kentli

Additional information is available at the end of the chapter

<http://dx.doi.org/10.5772/61130>

---

## Abstract

In this chapter, a power control system for a wound rotor induction generator has been explained. This power control system has realized a control method using a rotating reference frame fixed on the air-gap flux of the generator. Application of such a system allows control of the active and reactive power of generators independently and stably. So, a two-step process is presented here. The first step is to acquire the complex power expression (and thus the active and reactive power expressions) for an induction machine in space vector notation and in two-axes system. Then, a computer aided circuit is given to realize the power and current control by analyzing them. Also, the results of an experiment given in literature are shown to be able to compare the results.

**Keywords:** Doubly-fed wound rotor, Induction generator, Active and reactive power control

---

## 1. Introduction

Energy is defined as the capacity of a body to do mechanical work. Energy is preserved in earth in many different forms, such as solid (coal), liquid (petroleum), and gas (natural gas). Also, several resources are available such as solar, wind, wave, geothermal, and nuclear energy. On the other hand, energy cannot be found in nature in electrical form. However, electric energy has many advantages: easy to transmit at long distances and complying with customer's needs through adequate control.

More than 30% of energy is converted into electrical energy before usage by the help of electric generators that convert mechanical energy into electric energy [1]. There are two kinds of electric generators: synchronous generators and induction generators. Generally, synchronous generators are generally used in big power plants to produce electricity. On the other hand, induction generators are used in utilizing nonstable small energy resources such as uncontrollable and automatically load-regulated small running water and wind turbines (plants) [2, 3]. Wind turbines have become much more popular due to the increasing demand for clean energy. Due to expensive production and maintenance costs, multiwatt turbines/wind farms are preferred. Configurations of generators and their controllers differ. Squirrel cage generators, wound rotor generators, permanent magnet generators, DC generators, and variable reluctance generators are operated in these systems. But nowadays a kind of wound rotor, doubly-fed induction generator, has begun to be used more [4].

Both, the synchronous generator with rotating DC magnetic field and the induction generator, have similar fixed stator winding arrangement, which, when energized by a rotating magnetic field, produces a three-phase (or single phase) voltage output. However, the rotors of the two machines are quite different, with the rotor of an induction generator typically consisting of one of two types of arrangements: "squirrel cage" or a "wound rotor." Also, unlike the synchronous generator that has to be "synchronized" with the electrical grid before it can generate power, induction generator can be connected directly to the utility grid and driven directly by the turbines rotor blades at variable wind or running water speeds. Induction motor is an economical and reliable choice as generator in many wind and running water power turbines where its rotational speed, performance, and efficiency can be increased by coupling a mechanical gearbox.

Being cheap, reliable, and readily available in a wide power range from fractional horse power to multi-megawatt capacities leads squirrel cage induction motor type machines to be used in both domestic and commercial renewable energy/running water power applications. The features that make this motor desirable make also the induction generator desirable over other types of generators. Generally, induction generators are constructed based on the squirrel cage induction motor type.

However, the induction generator may provide the necessary power directly to the mains utility grid, but it also needs reactive power to its supply which is provided by the utility grid. Stand-alone (off-grid) operation of the induction generator is also possible but the disadvantage here is that the generator requires additional capacitors connected to its windings for self-excitation.

Three-phase induction machines are very well-suited for wind power and even hydroelectric (running water) generation. Induction machines, when functioning as generators, have a fixed stator and a rotational rotor, the same as that for the synchronous generator. However, excitation (creation of a magnetic field) of the rotor is performed differently and typical designs of the rotors are the squirrel-cage structure where conducting bars are embedded within the rotors' body and connected together at their ends by shorting rings and the wound (slip-ring) rotor structure that carries a normal 3-ph winding, connected in star or delta and terminated on three slip-rings, which are short-circuited when the machine is in normal operation.

Induction machines are also known as asynchronous machines, that is, they rotate below synchronous speed when used as a motor and above its synchronous speed by some prime mover when used as a generator. The prime mover may be a turbine, an engine, a windmill, or anything that is capable of supplying the torque and speed needed to drive the motor into the overspeed condition. So when rotated faster than its normal operating or no-load speed, induction generator produces AC electricity. In this position, the speed is hypersynchronous, the slip is negative (and usually small), the rotor e.m.f.s and currents have such direction as to demand active power output from the stator terminals. But magnetization is still dependent on the stator winding accepting reactive power for this purpose from the electrical source, so that the induction generator can only operate when connected to a live and synchronous AC system. If a lagging reactive power input is equated with a leading reactive power output, then the generator can be described as operating with a leading power factor. The torque acts in a direction opposite to that of the rotating field, requiring a mechanical drive at the shaft. Because an induction generator synchronizes directly with the main utility grid— that is, produces electricity at the same frequency and voltage – no rectifiers or inverters are required. A major advantage of the induction generator is frequency regulation. The output frequency and volts are regulated by the power system in the induction generators and are independent of speed variations. The self-regulation effect minimizes control system complexity. But the performance characteristics as a generator will vary slightly from those as a motor. In general, the slip rpm and power factor will be lower and the efficiency will be higher. The differences may be so insignificant as to be undetectable by normal field measuring methods. On the other hand, alongside advantages mentioned above of the squirrel-cage and wound rotor induction generators whose rotor windings are short-circuited, there are some disadvantages [2, 3]. For example, the active and reactive power of generators cannot be controlled independently and stably. A computer and a cycloconverter in rotor circuit are needed to accomplish this task.

In recent years, there has been an increased attention toward wind power generation. Conventionally, grid-connected cage rotor induction machines are used as wind generators at medium power level. When connected to the constant frequency network, the induction generator runs at near-synchronous speed drawing the magnetizing current from the mains, thereby resulting in constant-speed constant-frequency (CSCF) operation. However, the power capture due to fluctuating wind speed can be substantially improved if there is flexibility in varying the shaft speed. In such variable-speed constant-frequency (VSCF) application, rotor-side control of grid-connected wound rotor induction machine is an attractive solution [5]. A doubly-fed wound rotor induction generator can produce constant stator frequency even though rotor speed varies. This system can be controlled by a small-capacity converter compared with the generator capacity, when the control range speed is narrow. Because of these features, this system is currently considered to be adaptable to power systems for hydroelectric and wind-mill-type power plants [6-8].

When adapted to the power system, it is important to examine the effects of this system on the power system. In the system under consideration, the stator is directly connected to the three-phase grid and the rotor of the doubly-fed induction machine is excited by three-phase low-frequency AC currents, which are supplied via slip-rings by either a cycloconvert-

er or a voltage-fed PWM rectifier-inverter. The AC excitation on the basis of a rotor-position feedback loop makes it possible to achieve stable variable-speed operation. Adjusting the rotor speed makes the induction machine either release the electric power to the utility grid or absorb it from the utility grid [9]. The concept of power control was applied to reactive power compensator applications some 20 years ago, but the application to electrical machine control is new [10].

To control induction generator, several methods are used: electrically [vector control [11], active and reactive power control [12], direct torque control [13], direct power control [14], variable structure or sliding mode control [15], passivity control [16]], and mechanical (pitch, stall, and active stall control [17], yaw control [18], flywheel storage [9]). More information can be found in [19].

In literature, two kinds of approach are proposed for independent control of active and reactive powers. One of them is stator flux oriented vector control with rotor position sensors. The other is position sensorless vector control method. The control with rotor position sensors is the conventional approach and the performance of the system depends on the accuracy of computation of the stator flux and the accuracy of the rotor position information derived from the position encoder. Alignment of the position sensor is, moreover, difficult in a doubly-fed wound rotor machine [5].

Position sensorless vector control methods have been proposed by several research groups in the recent past [20-23]. A dynamic torque angle controller is proposed. This method uses integration of the PWM rotor voltage to compute the rotor flux; hence, satisfactory performance can not be achieved at or near synchronous speed. Most of the other methods proposed make use of the measured rotor current and use coordinate transformations for estimating the rotor position [21-23]. Varying degree of dependence on machine parameters is observed in all these strategies.

Alternative approaches to field-oriented control such as direct self control (DSC) and direct torque control (DTC) have been proposed for cage rotor induction machines. In these strategies, two hysteresis controllers, namely a torque controller and a flux controller, are used to determine the instantaneous switching state for the inverter. These methods of control are computationally very simple and do not require rotor position information. However, the application of such techniques to the control of wound rotor induction machine has not been considered so far. A recently developed algorithm for independent control of active and reactive powers with high dynamic response in case of a wound rotor induction machine is direct power control. In direct power control, the directly controlled quantities are the stator active and reactive powers. The proposed algorithm as direct power control also differs from DTC in that it does not use integration of PWM voltages. Hence, it can work stably even at zero rotor frequency. The method is inherently position sensorless and does not depend on machine parameters like stator/rotor resistance. It can be applied to VSCF applications like wind power generation as well as high-power drives [5].

Little literature has been published on control strategy and dynamic performance of doubly-fed induction machines [22; 24-27]. Leonhard (1985) describes a control strategy for an

adjustable-speed doubly-fed induction machine intended for independent control of the active and reactive power. The control strategy provides two kinds of current controllers: inner feedback loops of the rotor currents on the d-q coordinates and outer feedback loops of the stator currents on the M-T coordinates. However, it is not clarified theoretically why the control strategy requires the two kinds of current controllers.

This chapter describes the power control characteristics on the rotating reference frame fixed on the air-gap flux of a doubly-fed wound rotor induction generator and proposes a new approach to control with rotor position sensor. The proposed approach is the enhanced version of a previous study [28]. Thus, in this chapter, a new power control system that has been developed by using the computer and driver for a wound rotor induction generator takes place. This system is a new theoretical approach and this power control system has applied a control method using a rotating reference frame fixed on the air-gap flux of the generator. By using this control system, the active and reactive power of generator can be controlled independently and stably. Therefore, to achieve this purpose, firstly the complex power expression (and thus the active and reactive power expressions) for an induction machine in space vector notation and in two-axis system has been gotten. Then, power and current control, which are fundamental subjects, have been analyzed and as a result a computer- and driver-aided circuit is given to achieve the power and current control.

## 2. Analysis of the control system

For the stable control of the active and reactive power, it is necessary to independently control them. As known, the active power control is the control of torque produced by the machine and the reactive power control is the control of flux. The stator active and reactive power of doubly-fed wound rotor induction generator is controlled by regulating the current and voltage of the rotor windings. Therefore, to achieve independent control, the current and voltage of the rotor windings must be divided into components related to stator active and reactive power. It is well-known that an induction machine can be modeled as a voltage behind a total leakage inductance. Therefore, after a three-phase to two-phase variant transformation, the induction machine model becomes that of Fig. 1 [10].

Approximate vector diagram of an induction machine is shown in Fig. 2. In this section, the analysis of the doubly-fed wound rotor induction generator on the rotating frame fixed on the air-gap flux (M-T frame) is carried out.

The M-axis is fixed in the air-gap flux and the T-axis is fixed in the quadrature with the M-axis. The relations of stator  $\alpha_1$ - $\beta_1$  axis, rotor  $\alpha_2$ - $\beta_2$  axis, and M-T axis are shown in Fig. 3.

### 2.1. Complex power expression

Assuming that the voltage vector is used as the reference for the determination of lagging and leading, we can write the complex stator power expression for a machine in space vector notation as:

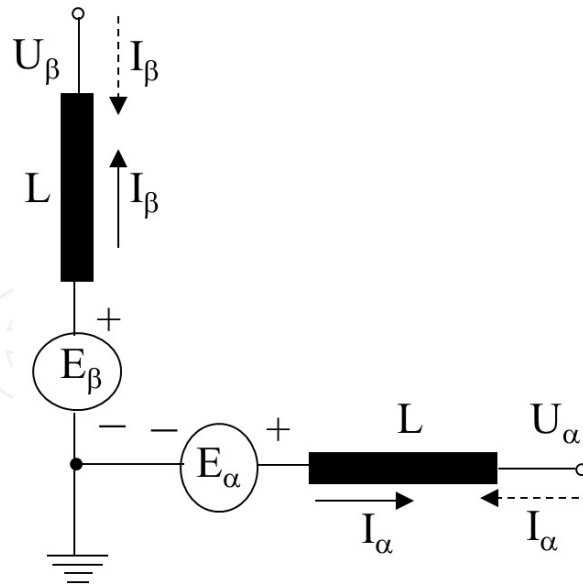


Figure 1. Two-phase representation of a three-phase induction machine (→generating; ← motoring)

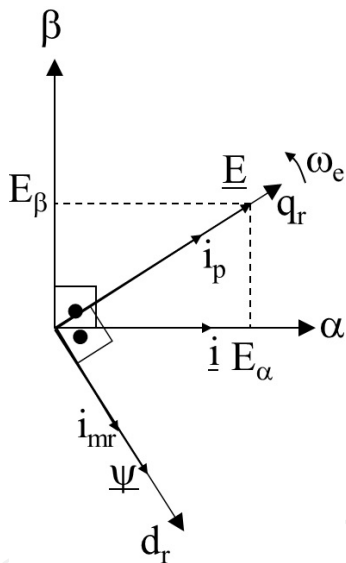


Figure 2. Approximate vector diagram of an induction machine

$$S_1 = I_1 \cdot U_1^* \tag{1}$$

which can be written in two-phase stationary frame variables as:

$$S_1 = [I_{M1,T1}] [U_{M1,T1}]^* \tag{2}$$

where

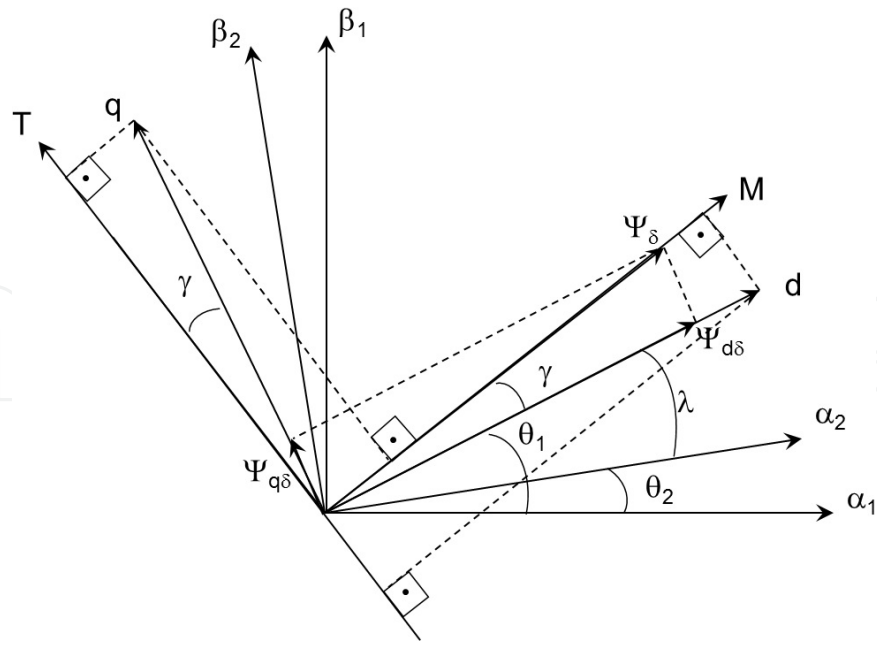


Figure 3. Vector diagram of M-T frame

$$[I_{M1,T1}] = I_{M1} + jI_{T1}; [U_{M1,T1}]^* = U_{M1} - jU_{T1}$$

Expanding Equation (2) we get the expressions for the stator active and reactive power as defined in [29]:

$$S_1 = U_{M1}I_{M1} + U_{T1}I_{T1} + j(U_{M1}I_{T1} - U_{T1}I_{M1}) \tag{3}$$

Therefore,

$$P_1 = U_{M1}I_{M1} + U_{T1}I_{T1} \tag{4}$$

$$Q_1 = U_{M1}I_{T1} - U_{T1}I_{M1} \tag{5}$$

where  $P_1$  is the stator active power, and  $Q_1$  is the stator reactive power,  $I_{M1}$  and  $I_{T1}$  are the M and T axis stator currents, and  $U_{M1}$  and  $U_{T1}$  are the M and T axis stator voltages.

## 2.2. Power control

In this section, the relationship between stator power and rotor current is analyzed. In Equations (4) and (5), the stator active and reactive power was expressed by the stator current based on the M-T frame. The relationships between the rotor and stator currents are:

$$I_{T1} = I_{q1} \cos \gamma - I_{d1} \sin \gamma \quad (6)$$

$$I_{T2} = I_{q2} \cos \gamma - I_{d2} \sin \gamma \quad (7)$$

$$I_{T1} + I_{T2} = (I_{q1} + I_{q2}) \cos \gamma - (I_{d1} + I_{d2}) \sin \gamma \quad (8)$$

$$I_{d1} = I_{M1} \cos \gamma; I_{d2} = I_{M2} \cos \gamma \quad (9)$$

$$I_{q1} = I_{M1} \sin \gamma; I_{q2} = I_{M2} \sin \gamma \quad (10)$$

$$I_{T1} + I_{T2} = 0; I_{T1} = -I_{T2} \quad (11)$$

By using Equations (9) and (10), the term of  $(I_{T1} + I_{T2})$  is expressed in terms of  $\psi_\delta$  and  $L_M$ :

$$I_{T1} + I_{T2} = \left( \frac{\psi_\delta}{L_M} \right) \sin \gamma \cos \gamma - \left( \frac{\psi_\delta}{L_M} \right) \cos \gamma \sin \gamma = 0 \quad (12)$$

$$\psi_\delta = L_M (I_{M1} + I_{M2}) \quad (13)$$

where  $\psi_\delta$  is the air-gap flux,  $I_{M2}$  and  $I_{T2}$  are the M and T axis rotor currents, and  $L_M$  is the mutual inductance.

By using Equations (12) and (13), the stator active and reactive power is expressed in terms of  $\psi_\delta$  and  $L_M$ :

$$P_1 = U_{M1} \left[ \left( L_M (I_{M1} + I_{M2}) / L_M \right) - I_{M2} \right] + U_{T1} (-I_{T2}) \quad (14)$$

$$P_1 = (\psi_\delta / L_M) U_{M1} - U_{M1} I_{M2} - U_{T1} I_{T2}$$

$$Q_1 = U_{M1} (-I_{T2}) - U_{T1} \left[ \left( L_M (I_{M1} + I_{M2}) / L_M \right) - I_{M2} \right] \quad (15)$$

$$Q_1 = U_{T1} I_{M2} - (\psi_\delta / L_M) U_{T1} - U_{M1} I_{T2}$$

In this system, the stator winding is directly connected to the power system. The conditions  $U_{M1} \approx 0$ ,  $U_{T1} \approx \text{constant}$ ,  $\psi_\delta \approx \text{constant}$  are derived from this feature [25]. By using these relationships and Equations (12), (13), (14), and (15), the stator active and reactive power is expressed in terms of rotor current. Equations (4) and (5) are rewritten as follows:

$$P_1 \approx -U_{T1} I_{T2} \quad (16)$$

$$Q_1 \approx U_{T1} I_{M2} - (\psi_\delta / L_M) U_{T1} \quad (17)$$

Equation (16) shows that the stator active power ( $P_1$ ) is expressed by the terms proportional to the rotor current  $I_{T2}$ . Equation (17) shows that the stator reactive power ( $Q_1$ ) is expressed by the terms proportional to the rotor current  $I_{M2}$  and constant value  $(\psi_\delta / L_M) U_{T1}$ . From the above relationships, the rotor current is divided into the active power ( $P_1$ ) and the reactive power ( $Q_1$ ) components. That is, the independent control of the stator active and reactive power can be actualized by regulating rotor currents  $I_{M2}$  and  $I_{T2}$ .

### 2.3. Current control

In this section, the relation between the rotor currents and the rotor voltages is analyzed. The equations for wound rotor induction machine based on M-T frame are shown as follows:

$$U_{M1} = R_1 I_{M1} + \frac{L_{1\sigma} dI_{M1}}{dt} - (\omega_1 + \omega_\delta) L_{1\sigma} I_{T1} + \frac{d\psi_{M1\delta}}{dt} - (\omega_1 + \omega_\delta) \psi_{T1\delta} \quad (18)$$

$$U_{T1} = R_1 I_{T1} + \frac{L_{1\sigma} dI_{T1}}{dt} + (\omega_1 + \omega_\delta) L_{1\sigma} I_{M1} + \frac{d\psi_{T1\delta}}{dt} + (\omega_1 + \omega_\delta) \psi_{M1\delta} \quad (19)$$

$$U_{M2} = R_2 I_{M2} + \frac{L_{2\sigma} dI_{M1}}{dt} - (\omega_s + \omega_\delta) L_{2\sigma} I_{T2} + \frac{d\psi_{M2\delta}}{dt} - (\omega_s + \omega_\delta) \psi_{T2\delta} \quad (20)$$

$$U_{T2} = R_2 I_{T2} + \frac{L_{2\sigma} dI_{T2}}{dt} + (\omega_s + \omega_\delta) L_{2\sigma} I_{M2} + \frac{d\psi_{T2\delta}}{dt} + (\omega_s + \omega_\delta) \psi_{M2\delta} \quad (21)$$

where  $\psi_{M1\delta}$  and  $\psi_{T1\delta}$  are the M and T axis stator air-gap flux,  $R_1$  and  $R_2$  are the stator and rotor resistance,  $\omega_1$  is the stator angular speed,  $\omega_\delta$  is the angular speed of the air-gap flux,  $\psi_{M2\delta}$  and  $\psi_{T2\delta}$  are the M and T axis rotor air-gap flux,  $L_{1\sigma}$  and  $L_{2\sigma}$  are the stator and rotor leakage inductance,  $\omega_s$  is the slip angular speed.

These equations are transformed by using the relationships  $\psi_{T1\delta} = \psi_{T2\delta}$ ,  $\psi_{M1\delta} = \psi_{M2\delta}$ , and  $\omega_s = \omega_1 - \omega_2$ , and the following expressions are derived:

$$U_{M2} = R_2 I_{M2} + \frac{L_{2\sigma} dI_{M2}}{dt} - (\omega_s + \omega_\delta) L_{2\sigma} I_{T2} + \frac{d\psi_{M1\delta}}{dt} - (\omega_s + \omega_\delta) \psi_{T2\delta} \quad (22)$$

$$U_{T2} = R_2 I_{T2} + \frac{L_{2\sigma} dI_{T2}}{dt} + (\omega_s + \omega_\delta) L_{2\sigma} I_{M2} + \frac{d\psi_{T1\delta}}{dt} + (\omega_s + \omega_\delta) \psi_{M2\delta} \quad (23)$$

$$U_{M2} = R_2 I_{M2} + \frac{L_{2\sigma} dI_{M2}}{dt} - (\omega_s + \omega_\delta) L_{2\sigma} I_{T2} + U_{M1\delta} + \omega_2 \psi_{T2\delta} \quad (24)$$

$$U_{T2} = R_2 I_{T2} + \frac{L_{2\sigma} dI_{T2}}{dt} + (\omega_s + \omega_\delta) L_{2\sigma} I_{M2} + U_{T1\delta} - \omega_2 \psi_{M2\delta} \quad (25)$$

where  $\omega_2$  is the rotor angular speed.

When the Equations (22), (23), (24), and (25) are transformed by the rotor current  $I_{M2}$  and  $I_{T2}$ , Equations (26) and (27) are given:

$$I_{M2} = (U_{M2} + (\omega_s + \omega_\delta) L_{2\sigma} I_{T2} - U_{M1\delta}) / (R_2 + pL_{2\sigma}) \quad (26)$$

$$I_{T2} = (U_{T2} - (\omega_s + \omega_\delta) L_{2\sigma} I_{M2} - U_{T1\delta} + \omega_2 \psi_\delta) / (R_2 + pL_{2\sigma}) \quad (27)$$

where  $p$  is the differential operator.

The stator winding is directly connected to the power system. Therefore, stator voltage becomes constant in the normal state, leading to the conditions  $U_{M1\delta} \approx 0$  and  $U_{T1\delta} \approx \text{constant}$ . And  $L_{2\sigma}$  is negligible because it is generally small [25].

Thus, Equations (26) and (27) become as follows:

$$I_{M2} = U_{M2} / R_2 \quad (28)$$

$$I_{T2} = (U_{T2} - U_{T1\delta} + \omega_2 \psi_\delta) / R_2 \quad (29)$$

Equations (28) and (29) show that rotor voltages along the M and T axes, respectively depend only on the rotor currents along the M and T axes. In other words, the relationships between the currents and voltages along the M and T axes are linear. Consequently, the rotor currents  $I_{M2}$  and  $I_{T2}$  can be controlled independently by regulating the rotor voltages  $U_{M2}$  and  $U_{T2}$ .

## 2.4. Composition of the control system

Figure 4 illustrates the control system diagram. Considering the analysis of control system, it can be interpreted that M-T frame can be used to describe the composition of the active and the reactive power. Mentioned control system has six parts: (1) power control loop (regulation of the rotor current references from the deviation between detection and reference values for both active and reactive power); (2) current PI regulator for rotor currents  $I_{M2}$  and  $I_{T2}$  (same application with the first part for regulation of the voltage); (3) air-gap flux calculator (using the stator currents, voltages, and the signals of the position sensor); (4)  $P_1$  and  $Q_1$  detector (calculation of the stator active and reactive power); (5) detector of the rotor current (vector values of M-T axis, Equation (30)); (6) coordinate transformer (three-phase voltage references, Equation (31)) [25].

$$\begin{bmatrix} I_{M2} \\ I_{T2} \end{bmatrix} = \begin{bmatrix} \cos(\lambda + \gamma) & \sin(\lambda + \gamma) \\ \sin(\lambda + \gamma) & \cos(\lambda + \gamma) \end{bmatrix} \begin{bmatrix} 1 & -1/2 & -1/2 \\ 0 & \sqrt{3}/2 & -\sqrt{3}/2 \end{bmatrix} \begin{bmatrix} I_{a2} \\ I_{b2} \\ I_{c2} \end{bmatrix} \quad (30)$$

$$\begin{bmatrix} U_{a2} \\ U_{b2} \\ U_{c2} \end{bmatrix} = \begin{bmatrix} 1 & 0 \\ -1/2 & \sqrt{3}/2 \\ -1/2 & -\sqrt{3}/2 \end{bmatrix} \begin{bmatrix} \cos(\lambda + \gamma) & -\sin(\lambda + \gamma) \\ \sin(\lambda + \gamma) & \cos(\lambda + \gamma) \end{bmatrix} \begin{bmatrix} U_{M2} \\ U_{T2} \end{bmatrix} \quad (31)$$

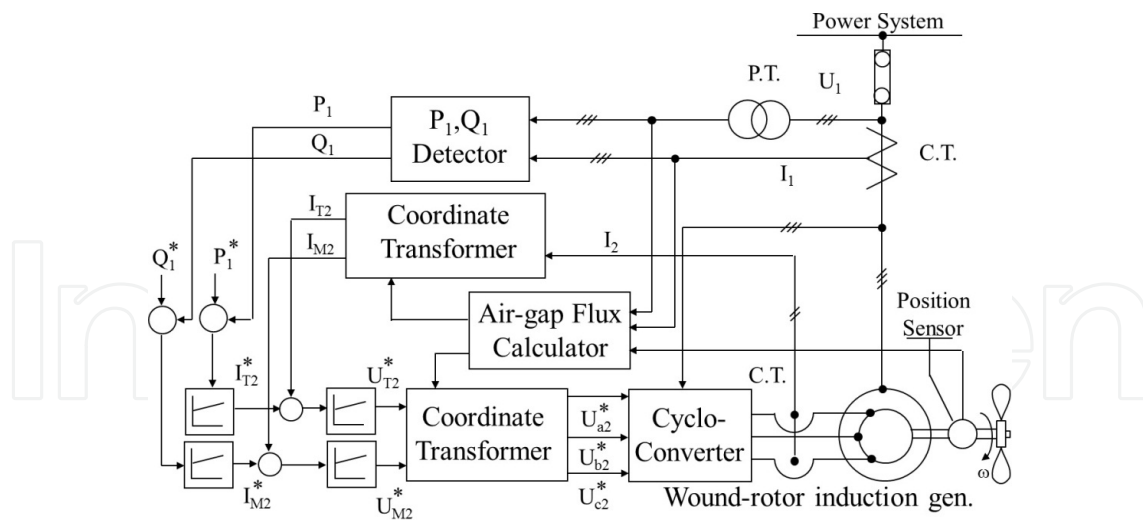


Figure 4. Block diagram of the control system

## 2.5. Power reference generation

Power Reference Generation (PRG) is one of the key modules of the algorithm. Strangely, it is the only module that depends on the parameter values. Due to direct connection to the torque,

active power reference is the simplest way to find out the torque value desired to produce. On the other hand, there are some difficulties related with the active power reference.

Normally, the following equation is enough to calculate active power reference [10]:

$$P_{ref} = T_{ref} \omega_{m2} = T_{ref} (2\pi n_2) \quad (32)$$

where  $T_{ref}$  is supplied from some outer loop such as a speed control loop, and  $n_2$  is the actual mechanical shaft speed at a particular instant of time.

Equation (32) is reliable under some limits so that calculated value of active power is not adequate to generate the torque  $T_{ref}$ . Main reason is the losses (losses in the stator and rotor resistance and iron losses) where all input power can not be transmitted to output. Loss in rotor resistance is influenced by the slip of the machine. Schematic demonstration of the power flows under motoring and generating for an induction machine are shown in Fig. 5.

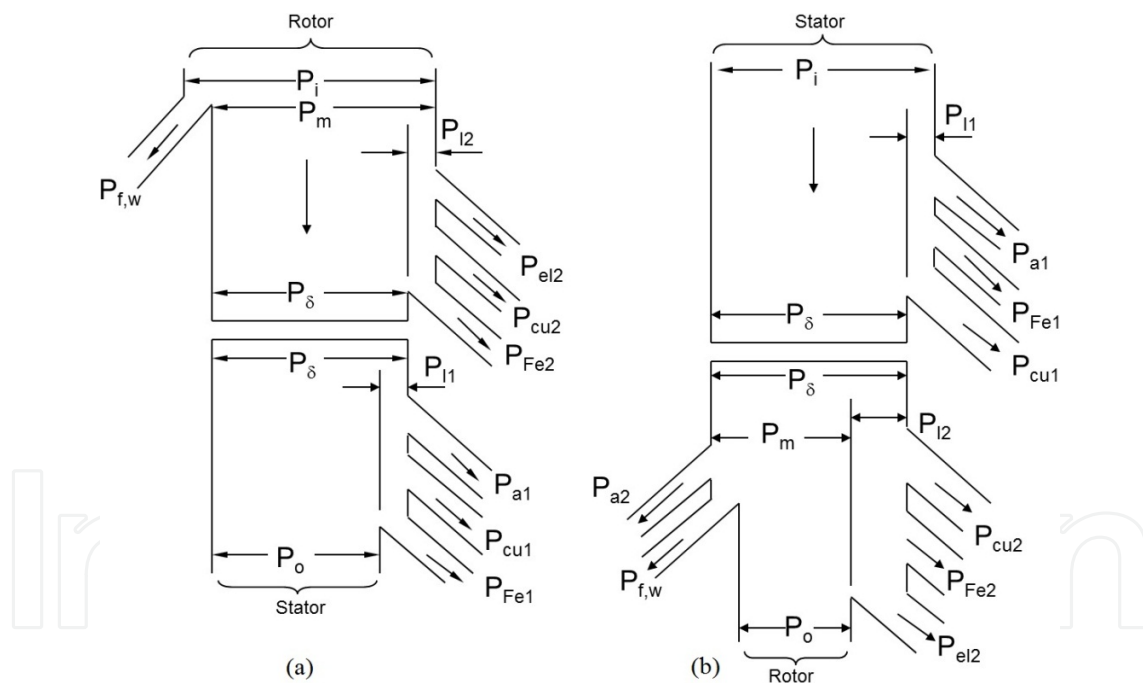


**Figure 5.** Schematic demonstration of the power flows in an induction machine under (a) motoring and (b) generating ( $P_i$  = input power (taken from supply in motor mode, given from shaft in generator mode),  $P_m$  = mechanical power,  $P_\delta$  = air-gap power (transferred from stator to rotor under motoring and from rotor to stator under generating),  $P_1$  = power loss,  $P_{fe}$  = iron loss,  $P_{cu}$  = copper loss,  $P_a$  = additional losses produced by harmonics,  $P_{f,w}$  = friction and windage losses,  $P_{el}$  = effective electrical power taken from rotor circuit,  $P_o$  = output power (shaft power in motor mode, electrical power in generation mode) (1 subscript means stator, 2 subscript means rotor) [28]

As seen in literature, whilst some researchers can assume that the stator resistance power and the iron losses can be ignored (under many practical situations), the power in the rotor

resistance cannot be ignored, especially under heavy load conditions when the slip of the machine can be large [10].

As the diagram shows, under the motoring condition the input power separates into two parts: one part is for the losses (stator, iron, and harmonics) and the other part is related with the rotating field power (air-gap power).

Also, under generating the input shaft power separates into two parts: the losses (friction, windage) and mechanical power. All these parts should be balanced to reach the goal power value. To manage this aim, we should be able to calculate the slip and afterward we could calculate required power expressions as follows for the motoring/generating situation (if the friction and windage losses are neglected):

$$P_{ref} = \frac{P_{shaft}}{(1-s)} = \frac{T_{ref} \omega_{m2}}{(1-s)} \quad (33)$$

where  $P_{shaft}$  is the desired shaft power, and  $P_{ref}$  is the terminal reference power as defined previously.

The reactive power reference generation is linked with the slip. So, first we should deal with it. Figure 2 gives an approximate vector diagram of the voltages, currents, and fluxes of an induction machine. Reactive power can be calculated as the multiplication of the emf voltage  $E$  in one axis (e.g.  $q_r$ ) of the machine by the current in the other axis (e.g.  $d_r$ ):

$$|Q| = I_{mr} E \quad (34)$$

$$|Q| = I_{mr} \omega_1 \psi_m \quad (35)$$

where  $\psi_m$  is the flux magnitude,  $I_{mr}$  is the magnetising current, and  $\omega_1$  is the stator angular speed related with electrical frequency.

Rearranging (35) one can write:

$$\omega_{sref} = - \left( \frac{|Q_{ref}|}{(I_{mrref} \psi_{mref})} \right) - \omega_2 \quad (36)$$

realizing:

$$f_2 = p_p \cdot n_2$$

$$\omega_2 = p_p \cdot \omega_{m2}$$

$$\omega_1 = \omega_2 + \omega_s$$

$\omega_s$  = slip angular speed related with slip frequency

$\omega_{s\text{ref}}$  = the desired slip angular speed related with slip frequency

$I_{mr\text{ref}}$  = the desired magnetizing current

$p_p$  = the pole pairs

$|Q_{ref}|$  = the desired reactive power

The negative sign in Equation (36) results from the sign of  $Q_{ref}$ , the reference reactive power.

Given Equation (36), we can now write the expression for the slip:

$$s = \frac{\omega_s}{(\omega_2 + \omega_s)} = 1 + \left( \omega_2 I_{mr\text{ref}} \psi_{m\text{ref}} / Q_{ref} \right) = 1 + \left( \omega_2 L_m I_{mr\text{ref}}^2 / Q_{ref} \right) \quad (37)$$

This expression can be substituted into the active power slip compensation term  $1/(1-s)$ . The  $I_{mr\text{ref}}$  and  $\psi_{m\text{ref}}$  terms in this expression are reference values. Clearly,  $I_{mr}$  and  $\psi_m$  for an induction machine are related, that is,  $\psi_m = L_m \cdot I_{mr}$ . Hence, we have written the numerator of Equation (37) as  $L_m \cdot I_{mr\text{ref}}^2$ . This requires acquiring the value of magnetizing inductance of the machine.

The reactive power expression can be written as:

$$|Q_{ref}| = I_{mr} \omega_1 \psi_m = I_{mr} \psi_m (\omega_2 + \omega_s) \quad (38)$$

So, it can be concluded that the reactive power is dependent on the slip frequency. The slip frequency is well-related with the torque. In case a rapid change in torque is needed, slip frequency changes as a step and consequently the reactive power value changes. The torque  $T$  and  $\omega_s$  expressions of an induction machine can be written as (using the standard expression from Field Oriented Control):

$$T = 1.5 p_p L_m^2 |I_{mr}| I_p / L_2 \quad (39)$$

$$\omega_s = I_p / (\tau_2 |I_{mr}|) \quad (40)$$

where  $\tau_2 = L_2 / R_2$ ,  $L_2$  = the rotor inductance, and  $R_2$  = the rotor resistance. Therefore,  $\tau_2$  is the rotor time constant.

Rearranging Equation (39), one can write:

$$I_p = (TL_2) / (1.5p_p L_m^2 |I_{mr}|) \tag{41}$$

Substituting Equation (41) into Equation (40) gives:

$$\omega_s = (TL_2) / (1.5p_p L_m^2 |I_{mr}|^2 \tau_2) \tag{42}$$

The denominator in Equation (42) can be simplified by assuming that the leakage inductance of the machine is very small in relation to  $L_2$ , and hence  $L_2 \approx L_m$ . Therefore, Equation (42) can be written as:

$$\omega_s \approx \frac{2T}{(3p_p L_m |I_{mr}|^2 \tau_2)} = \frac{2T}{(3p_p \psi_m |I_{mr}| \tau_2)} \tag{43}$$

We are now in a position to write an expression for the reference reactive power. Substituting Equation (43) into Equation (38) and simplifying, we get Equation (44):

$$Q_{ref} = - \left[ (|I_{mr}|_{ref} \omega_2 \psi_{mref}) + \left( \frac{2T_{ref}}{3p_p \tau_2} \right) \right] = - \left[ L_m (|I_{mr}|_{ref})^2 \omega_2 + \left( \frac{2T_{ref}}{3p_p \tau_2} \right) \right] \tag{44}$$

### 3. Experimental studies

An experimental setup using the control system shown in Fig. 4 was established by Yamamoto and Motoyoshi and the characteristics of the control system along the M-T frame have been experimentally examined. Experimental data are taken from their study [25]. The schematic diagram of the experimental system is shown in Fig. 6. Specifications of the generator used in experimental system are shown in Table 1. Equations (16) and (17) show that active and reactive power is proportional to the rotor currents  $I_{T2}$  and  $I_{M2}$ .

|                |       |                   |          |
|----------------|-------|-------------------|----------|
| Phase          | 3     | Stator Voltage    | 270 V    |
| Pole Pairs     | 2     | Rotor Voltage     | 257 V    |
| Power Capacity | 20 kW | Synchronous Speed | 1500 rpm |

Table 1. Specifications of the generator used in experimental system [25]

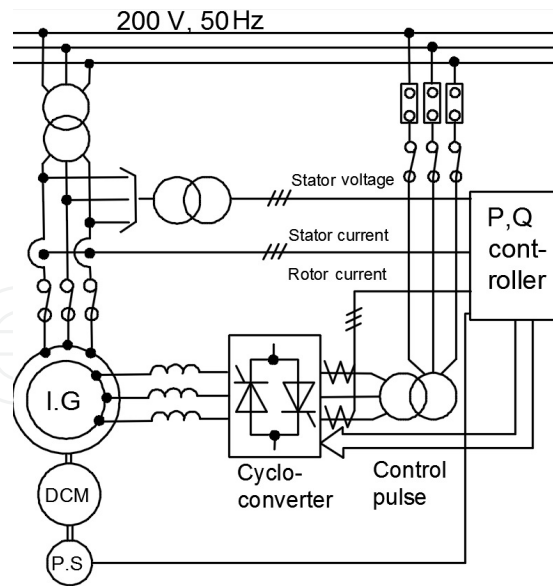


Figure 6. Experimental system [25]

### 3.1. Experimental results

Figures 7 and 8 show the relationships between stator power and rotor current reference and Figs. 9 and 10 show the relationships between stator power and stator power reference.

Figure 10 shows the step response of the stator reactive power  $Q_1$  and the step response of the rotor current  $I_{M2}$  which is in proportion to the stator reactive power ( $Q_1$ ). Figure 8 shows the step response of the rotor current  $I_{T2}$  which is in proportion to the stator active power ( $P_1$ ). Figure 9 shows the step response of the stator active power  $P_1$ .  $I_{M2}$  and  $I_{T2}$  respond to stepping of  $I_{M2}^*$  and  $I_{T2}^*$  in 20 ms without any effect on  $I_{T2}$  and  $I_{M2}$ .  $P_1$  and  $Q_1$  respond to stepping of  $P_1^*$  and  $Q_1^*$  in 80 ms without any effect on  $Q_1$  and  $P_1$ . The effects of this active and reactive power control method have been proved by these experimental results.

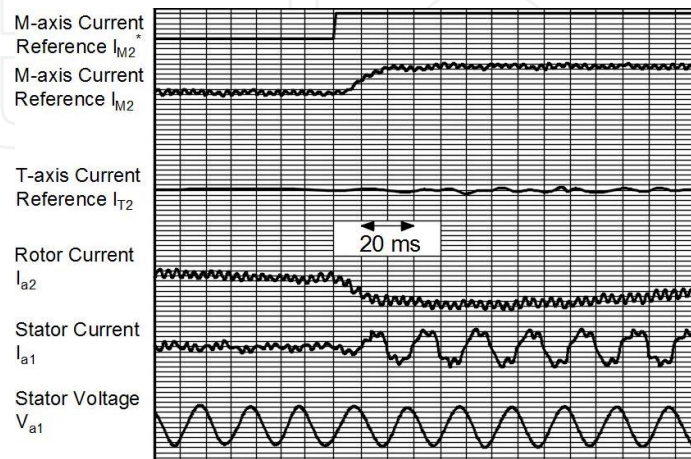


Figure 7. Step response of the M-axis current [25]

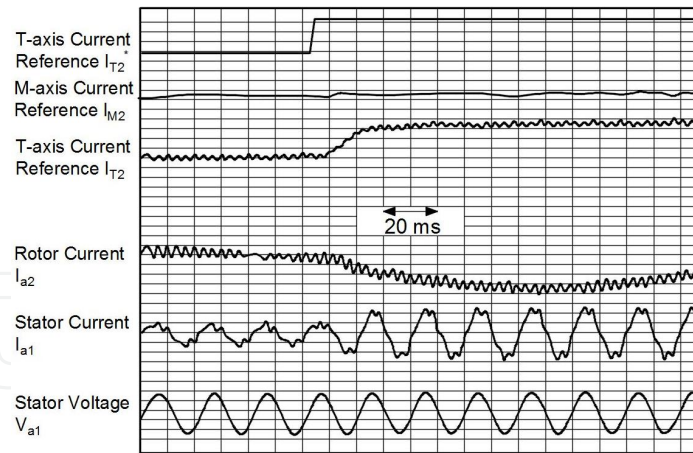


Figure 8. Step response of the T-axis current [25]

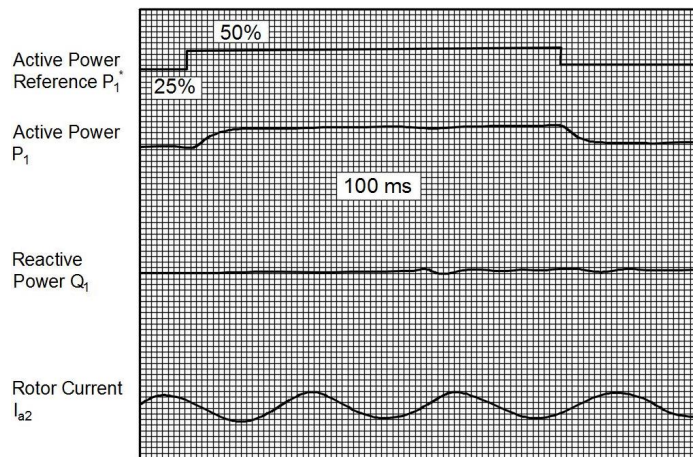


Figure 9. Step response of the active power [25]

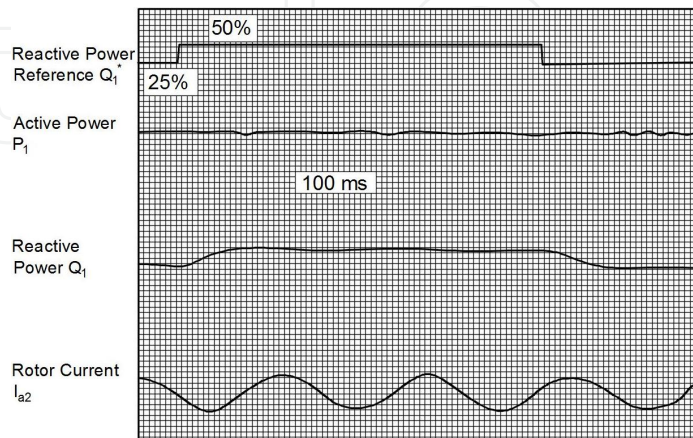


Figure 10. Step response of the reactive power [25]

### 3.2. Harmonic analysis

For the power converter of this system, the cycloconverter which is suitable for a large capacity system is often used. Generally, when the large-scale converter is applied to the electric power network system, it is a very important item to analyze the harmonic currents of the power converter. As known, the harmonic currents of the power converter are transmitted to the electric power network system through the rotor and stator windings. In this chapter, the characteristics of the transmission of the harmonic currents caused by the cycloconverter are analyzed theoretically.

Before beginning analysis, let us remember the basic principles of cycloconverter and mathematical background (taken from [30]) for the understanding of the subject.

#### 3.2.1. Principle of the cycloconverter

As known, cycloconversion is concerned mostly with direct conversion of energy to a different frequency by synthesizing a low-frequency wave from appropriate sections of a higher-frequency source. As shown in Fig. 11a, a cycloconverter can be considered to be composed of two converters connected back-to-back. The load waveforms of Fig. 11b show that in the general case, the instantaneous power flows in the load fall into one of four periods. The two periods, when the product of load voltage and current is positive, require power flow into the load, dictating a situation where the converter groups rectify, the positive and negative groups conducting respectively during the appropriate positive and negative load-current periods.

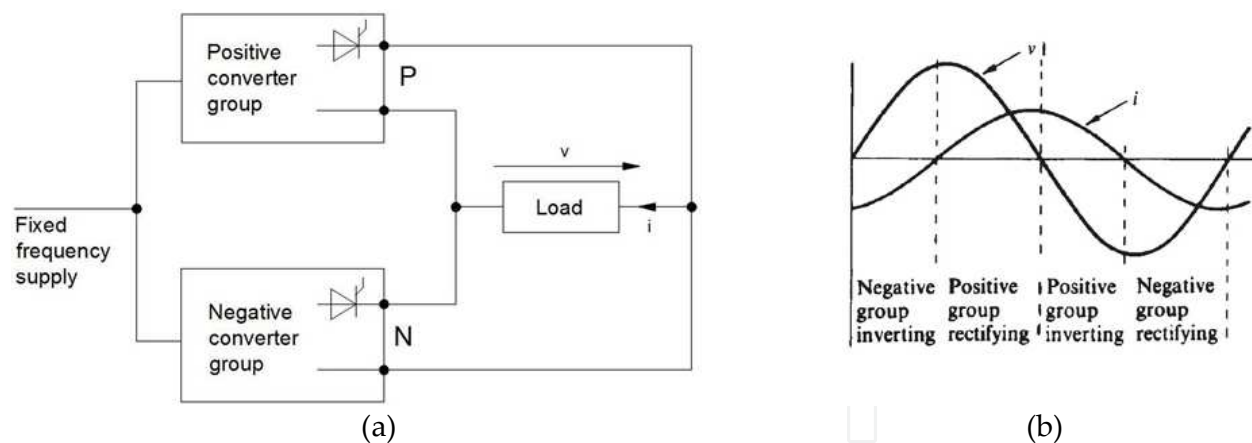


**Figure 11.** General cycloconverter layout (a) Block diagram representation, (b) Ideal load waveforms [30]

The other two periods represent times when the product of load voltage and current is negative; hence, the power flow is out of the load, demanding that the converters operate in the inverting mode. As shown in Fig. 11a, the principle of the cycloconverter can be demonstrated by using the simplest possible single-phase input to single-phase output with a pure resistance as load. Each converter is a bi-phase half-wave connection, the positive group labeled P and the negative group for reverse current labeled N.

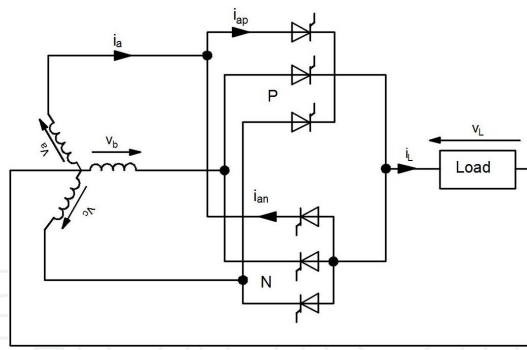


Figure 12. Single-phase load fed from a three-pulse cycloconverter [30]

The operation of the blocked group cycloconverter with various loads can be readily explained by reference to the three-pulse connection shown in Fig. 12, with the associated waveforms for inductive load in Figs. 13 and 14. As known, the wound rotor induction motor is an inductive load. In this chapter, waveforms are drawn for inductive load.

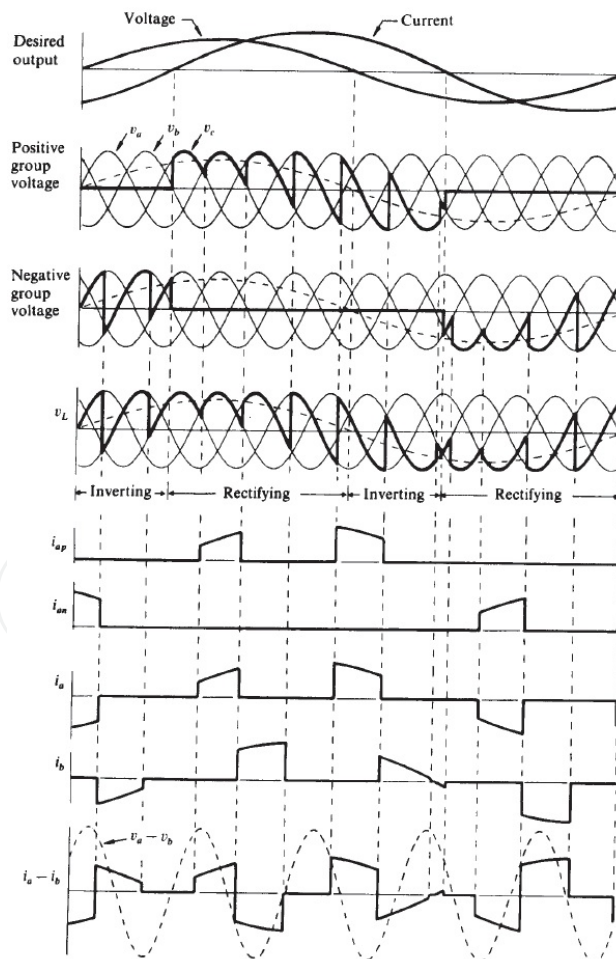


Figure 13. Waveforms with maximum voltage to an inductive load [30]

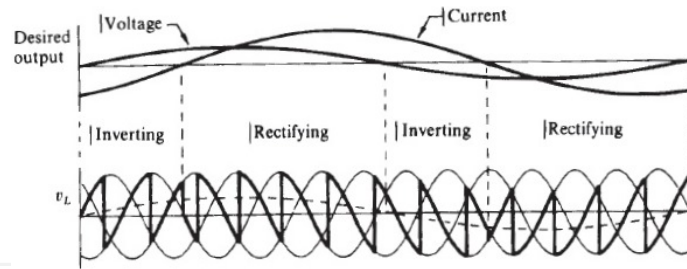


Figure 14. Waveforms when the load voltage is at half maximum (inductive load current continuous) [30]

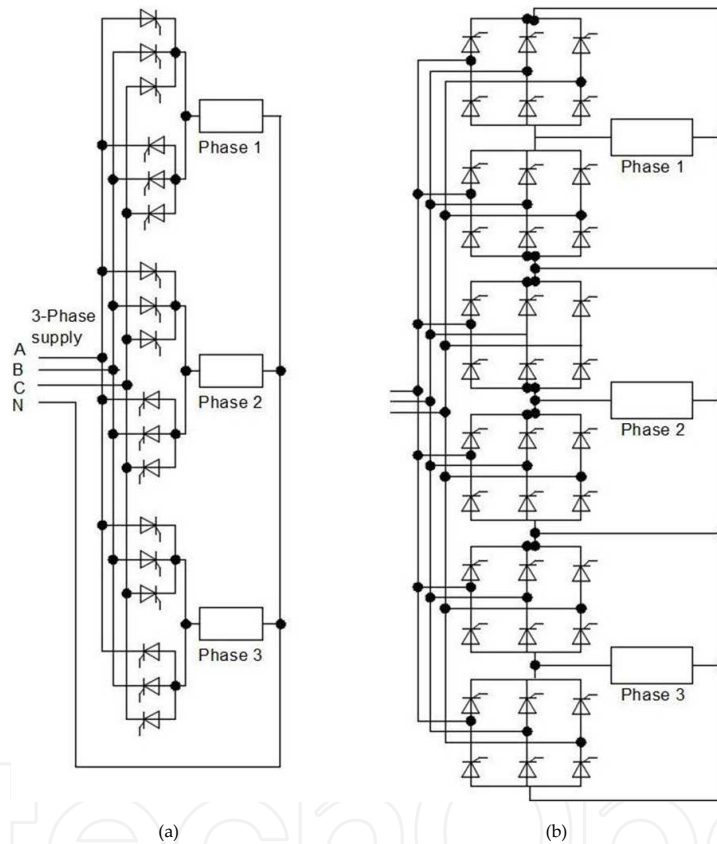


Figure 15. Cycloconverter connections with three-phase output. (a) Three-pulse bridge, (b) Six-pulse bridge [30]

The waveforms are as shown in Fig. 13 when the load is inductive, these being at a condition of maximum voltage. The load current will lag the voltage and, as the load-current direction determines which group is conducting, the group on-periods are delayed relative to the desired output voltage. The group thyristors are fired at such angles to achieve an output as close as possible to a sinewave, but now the lagging load current takes each group into the inverting mode. The group will cease conducting when the load current reverses. The load-voltage waveform is shown as a smooth transfer between groups, but in practice, a short gap would be present to ensure cessation of current in, and the regaining of the blocking state in, the outgoing group, before the incoming group is fired. The waveforms drawn assume the

current is continuous within each load half-cycle. The effects of overlap will in practice be present in the waveforms.

In practice, the load-current waveform in Fig. 13 is assumed to be sinusoidal, although it would contain a ripple somewhat smaller than that in the voltage waveform. A light load inductance would result in discontinuous current, giving short zero-voltage periods. Each thyristor will conduct the appropriate block of load current, having the branch currents shown. The current  $i_a - i_b$  would represent the transformer input line current if one assumed the supply to be via a delta primary transformer. The input-current waveform shows changes in shape from cycle to cycle but where the input and output frequencies are an exact multiple, the waveform will repeat over each period of output frequency.

As shown in Fig. 14, a reduction in the output voltage can be obtained by firing angle delay. Here firing is delayed, even at the peak of the output voltage, so that control is possible over the magnitude of the output voltage. Comparison of Fig. 14 with Fig. 13 indicates a higher ripple content when the output voltage is reduced.

As shown in Fig. 15a, the three-pulse cycloconverter when feeding a three-phase load can be connected with a total of 18 thyristors. As shown in Fig. 15b, a six-pulse cycloconverter can be based on either six-phase half-wave blocks or the bridge connection when 36 thyristors are required.

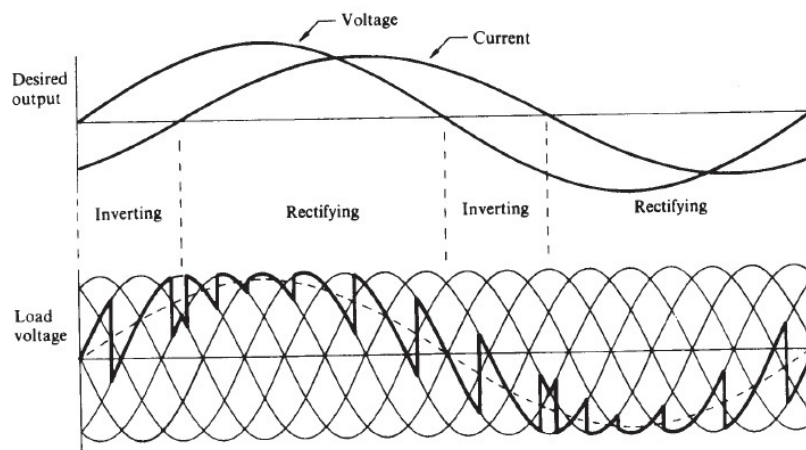


**Figure 16.** Cycloconverter load-voltage waveform with a lagging power factor load (six-pulse connection) [30]

An example of the cycloconverter output waveforms for the higher-pulse connections is given in Fig. 16, with an output frequency of one-third of the input frequency. It is clear from these waveforms that the higher the pulse-number, the closer is the output waveform to the desired sinusoidal waveform. In general, the output frequency is in general limited to about one-half to one-third of the input frequency, the higher-pulse connections permitting a higher limit.

As in Fig. 15, when the three-pulse cycloconverter feeds a three-phase balanced load, the current loading on the supply is much more evenly balanced. The waveforms to illustrate this are given in Fig. 17 for a frequency ratio of 4/1 with a load of 0.707 power factor lagging. It has

been assumed that the load current is sinusoidal, although in practice it must contain ripple. The total load current is not identical from one cycle to the next, obviously contains harmonics, and its fundamental component lags the supply voltage by a larger amount than the load power factor angle.

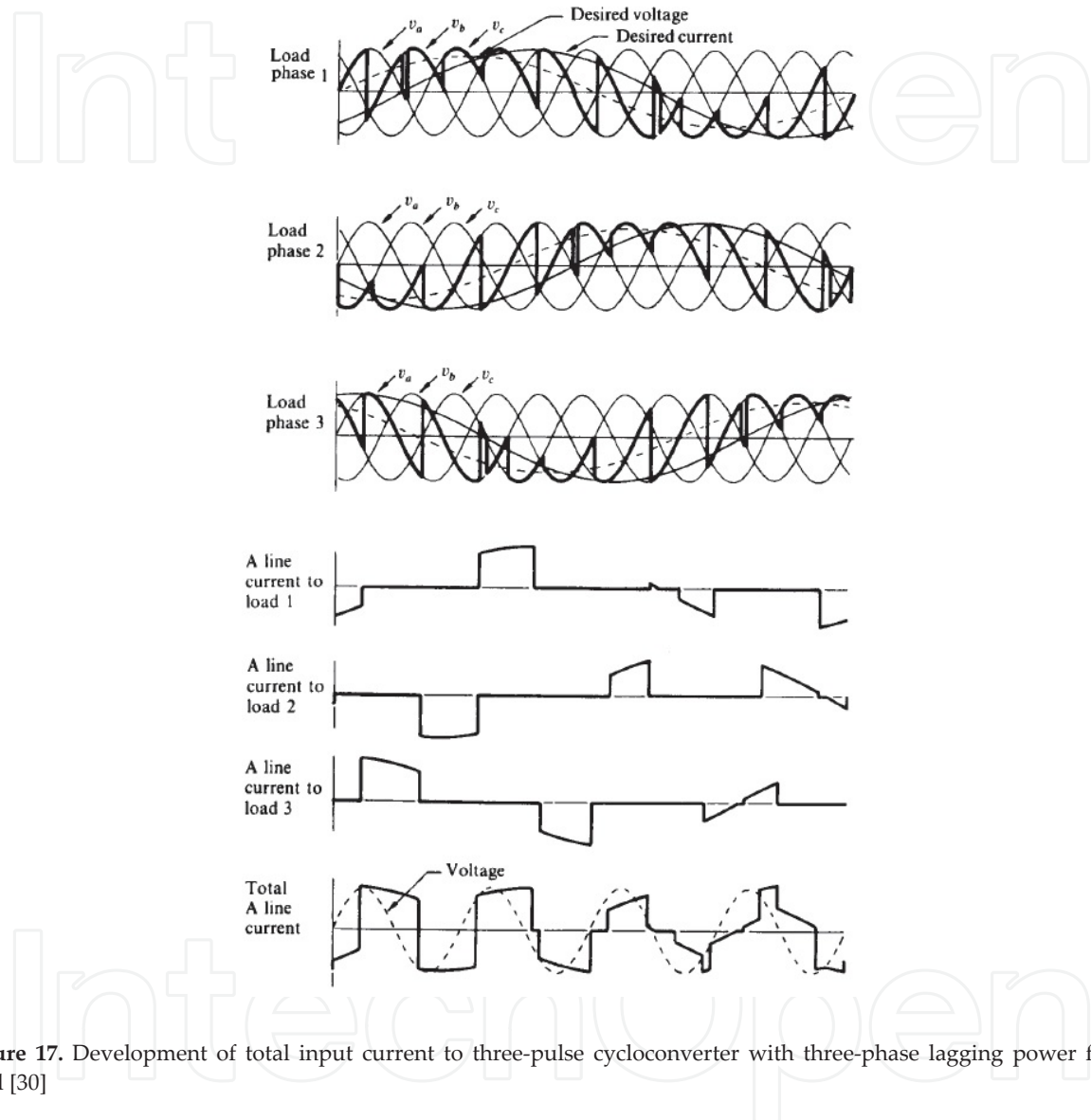


**Figure 17.** Development of total input current to three-pulse cycloconverter with three-phase lagging power factor load [30]

The thyristors of a cycloconverter are commutated naturally, and whether the load is resistive, inductive, or capacitive, the firing of the thyristors must be delayed to shape the output. The net result is that the AC supply input current will always lag its associated voltage.

### 3.2.2. Circulating current mode

The previous section specified cycloconverter operation where either the positive or negative groups were conducting, but never together. As shown in Fig. 18, if a center-tapped reactor is connected between the positive group P and negative group N, then both groups can be

permitted to conduct. The reactor will limit the circulating current, that is, the value of its inductance to the flow of load current from either group being one quarter of its value to the circulating current, because inductance is proportional to the square of the number of turns.

In Fig. 19, typical waveforms are shown for the three-pulse cycloconverter shown in Fig. 18. Each group conducts continuously, with rectifying and inverting modes as shown. The mean between the two groups will be fed to the load, some of the ripple being cancelled in the combination of the two groups. Both groups synthesize the same fundamental sinewave. The reactor voltage is the instantaneous difference between the two group voltages. The circulating current shown in Fig. 19 can only flow in one direction, the thyristors preventing reverse flow. Hence, the current will build up during the reactor voltage positive periods until in the steady state it is continuous, rising and falling as shown.

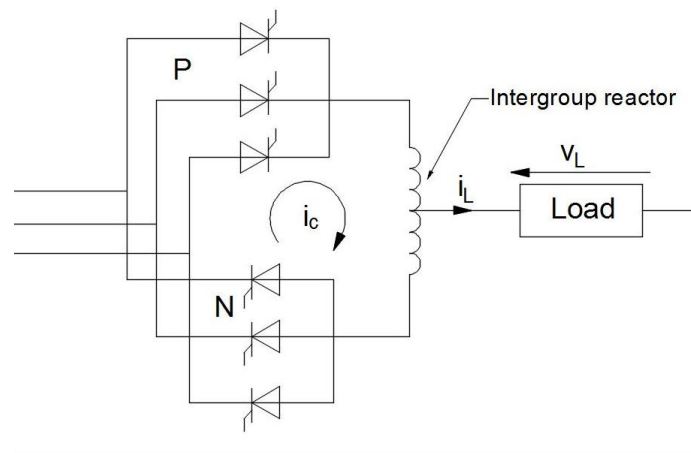


**Figure 18.** Three-pulse cycloconverter with intergroup reactor [30]

### 3.2.3. Mathematical analysis

The above subjects have demonstrated that almost all the waveforms associated with power electronic equipment are non-sinusoidal, which contains harmonic components. The purpose of this subject is to analyze the harmonic content of the various waveforms and discuss their effects as regards both supply and load.

Any periodic waveform may be shown to be composed of the superposition of a direct component with a fundamental pure sinewave component, together with pure sinewaves known as harmonics at frequencies which are integral multiples of the fundamental. A non-sinusoidal wave is often referred to as a complex wave [30].

Mathematically, it is more convenient to express the independent variable as  $x$  and the dependent variable as  $y$ . Then, the series may be expressed as:

$$y = f(x) = a_0 + a_1 \cos(x) + a_2 \cos(2x) + \dots + a_n \cos(nx) + b_1 \sin(x) + b_2 \sin(2x) + \dots + b_n \sin(nx) \quad (45)$$

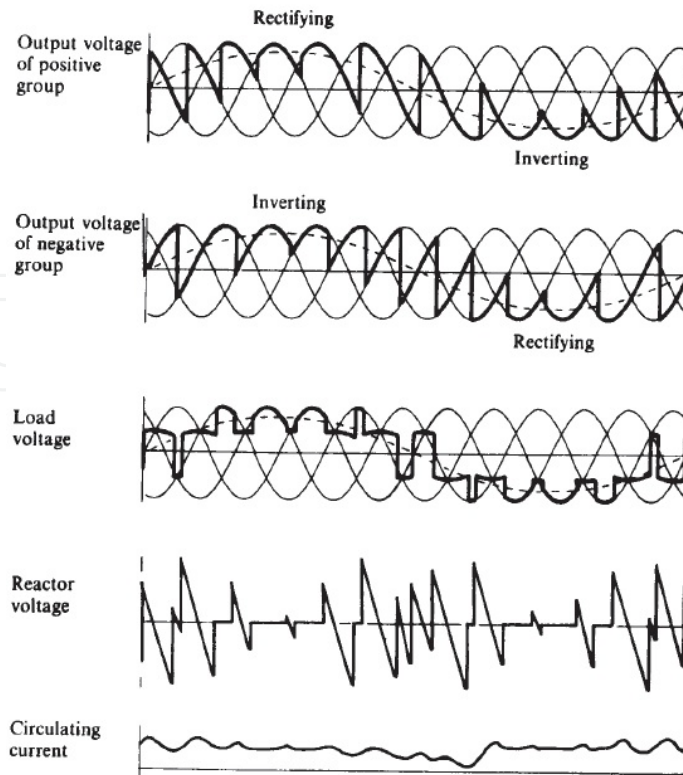


Figure 19. Waveform of a three-pulse cycloconverter with circulating current but without load [30]

Equation (45) is known as a Fourier series, and where  $f(x)$  can be expressed mathematically, a Fourier analysis yields that the coefficients are [31]:

$$a_0 = \frac{1}{2\pi} \int_{-\pi}^{\pi} f(x) dx \tag{46}$$

$$a_n = \frac{1}{\pi} \int_{-\pi}^{\pi} f(x) \cos nx dx \tag{47}$$

$$b_n = \frac{1}{\pi} \int_{-\pi}^{\pi} f(x) \sin nx dx \tag{48}$$

Alternatively, the series may be expressed as:

$$y = f(x) = R_0 + R_1 \sin(x - \phi_1) + R_2 \sin(2x - \phi_2) + R_3 \sin(3x - \phi_3) + \dots + R_n \sin(nx - \phi_n) \tag{49}$$

Equations (49) and (45) are equivalent, with:

$$a_n \cos nx + b_n \sin nx = R_n \sin(nx - \phi_n) \quad (50)$$

From which the resultant and phase angle:

$$R_n = (a_n^2 + b_n^2)^{1/2} \quad (51)$$

$$\phi_n = \arctan \frac{a_n}{b_n} \quad (52)$$

Electrically, it expresses the independent variable as  $\omega t$  instead of  $x$  and the dependent variable as volts or amperes instead of  $y$ . Then, the series may be expressed as:

$$v = V_0 + V_1 \sin(\omega t - \phi_1) + V_2 \sin(2\omega t - \phi_2) + V_3 \sin(3\omega t - \phi_3) + \dots + V_n \sin(n\omega t - \phi_n) \quad (53)$$

where

$v$  is the instantaneous value of the voltage at any time  $t$ ;

$V_0$  is the direct (or mean) value of the voltage;

$V_1$  is the maximum value of the fundamental component of the voltage;

$V_2$  is the maximum value of the second harmonic component of the voltage;

$V_3$  is the maximum value of the third harmonic component of the voltage;

$V_n$  is the maximum value of the  $n$ th harmonic component of the voltage;

$\phi$  defines the relative angular reference; and

$\omega = 2\pi f$ , where  $f$  is the frequency of the fundamental component,  $1/f$

defining the time over which the complex wave repeats itself.

The constant term of Equation (46) is the mean value of the function, and is the value found in, for example, the calculation of the direct (mean) voltage output of a rectifier. In the analysis of a complex wave, certain statements and simplifications are possible by inspection of any given waveform. If the areas of the positive and negative half-cycles are equal, then  $a_0$  is zero. If  $f(x + \pi) = -f(x)$ , then there are no even harmonics, that is, no second, fourth, etc. In plain terms, this means the negative half-cycle is a reflection of the positive half-cycle. If  $f(-x) = -f(x)$ , then  $a_n = 0$ ; that is, there are no sine terms. If  $f(-x) = f(x)$ , then  $b_n = 0$ ; that is, there are no cosine terms. Symmetry of the waveform can result in Equations (47) and (48) being taken as twice the value of the integral from 0 to  $\pi$ , or four times the value of the integral from 0 to  $\pi/2$ , hence simplifying the analysis.

Where it is difficult to put a mathematical expression to  $f(x)$ , or where an analysis of an experimental or practical waveform obtained from a piece of equipment is required, graphical analysis can be performed [30].

The conditions of analysis are as follows.

1. The frequency of the harmonic current for the three-pulse and six-pulse cycloconverter is  $6mfl \pm (2n + 1)fs$ , where  $m$  is any integer from 1 to infinity,  $n$  is any integer from 0 to infinity,  $fl$  is the frequency of the power source, and  $fs$  is the output frequency of the cycloconverter [32].
2. The analysis is carried out only on the harmonic components.
3. Zero-phase-sequence current (harmonic currents of multiple of 3) is neglected.
4. The stator is connected to the fundamental frequency voltage source.

Using these conditions, the three-phase rotor current can be defined as follows:

$$I_{a2} = \sum_m \sum_n A_{(6n-1)m} \text{Sin}\{6m\theta_1 - (6n-1)\theta_s\} + A_{(6n-5)m} \text{Sin}\{6m\theta_1 - (6n-5)\theta_s\} + B_{(6n-1)m} \text{Sin}\{6m\theta_1 - (6n-1)\theta_s\} + B_{(6n-5)m} \text{Sin}\{6m\theta_1 - (6n-5)\theta_s\} \quad (54)$$

$$I_{b2} = \sum_m \sum_n A_{(6n-1)m} \text{Sin}\left\{6m\theta_1 - (6n-1)\left(\theta_s - \frac{2\pi}{3}\right)\right\} + A_{(6n-5)m} \text{Sin}\left\{6m\theta_1 - (6n-5)\left(\theta_s - \frac{2\pi}{3}\right)\right\} + B_{(6n-1)m} \text{Sin}\left\{6m\theta_1 - (6n-1)\left(\theta_s - \frac{2\pi}{3}\right)\right\} + B_{(6n-5)m} \text{Sin}\left\{6m\theta_1 - (6n-5)\left(\theta_s - \frac{2\pi}{3}\right)\right\} \quad (55)$$

$$I_{c2} = \sum_m \sum_n A_{(6n-1)m} \text{Sin}\left\{6m\theta_1 - (6n-1)\left(\theta_s + \frac{2\pi}{3}\right)\right\} + A_{(6n-5)m} \text{Sin}\left\{6m\theta_1 - (6n-5)\left(\theta_s + \frac{2\pi}{3}\right)\right\} + B_{(6n-1)m} \text{Sin}\left\{6m\theta_1 - (6n-1)\left(\theta_s + \frac{2\pi}{3}\right)\right\} + B_{(6n-5)m} \text{Sin}\left\{6m\theta_1 - (6n-5)\left(\theta_s + \frac{2\pi}{3}\right)\right\} \quad (56)$$

where  $m=1,2,\dots, n=1,2,\dots, \theta_1=\omega_1 t$ ;  $\omega_1$  is the stator angular speed,  $\theta_s=\omega_s t$ ;  $\omega_s$  is the slip angular speed.

When Equations (54)–(56) are transformed to the d-q axis based on the stator voltage, (57) and (58) are derived:

$$I_{d2} = \sum_m \sum_n \begin{aligned} & A_{(6n-1)m} \text{Sin}\{6m\theta_1 - 6n\theta_s\} \\ & + A_{(6n-5)m} \text{Sin}\{6m\theta_1 - (6n-1)\theta_s\} \\ & + B_{(6n-1)m} \text{Sin}\{6m\theta_1 + 6n\theta_s\} \\ & + B_{(6n-5)m} \text{Sin}\{6m\theta_1 + (6n-1)\theta_s\} \end{aligned} \quad (57)$$

$$I_{q2} = \sum_m \sum_n \begin{aligned} & A_{(6n-1)m} \text{Cos}\{6m\theta_1 - 6n\theta_s\} \\ & + A_{(6n-5)m} \text{Cos}\{6m\theta_1 - (6n-1)\theta_s\} \\ & + B_{(6n-1)m} \text{Cos}\{6m\theta_1 + 6n\theta_s\} \\ & + B_{(6n-5)m} \text{Cos}\{6m\theta_1 + (6n-1)\theta_s\} \end{aligned} \quad (58)$$

The characteristics of transmission from the rotor winding to the stator winding are analyzed by substituting into the fundamental equation of a wound rotor induction machine. The analysis uses the symmetrical coordinate method for simplification. In this case, positive phase sequence component value (F component value) and negative phase sequence component value (B component value) have a conjugate relationship. The F component value is used for the analysis in this paper, which gives the following fundamental equation of the wound rotor induction machine:

$$\begin{bmatrix} V_{F1} \\ V_{F2} \end{bmatrix} = \begin{bmatrix} R_1 + (p + j\omega_1)(L_1 + L_m) & (p + j\omega_1)L_m \\ (p + j\omega_0)L_m & R_2 + (p + j\omega_0)(L_2 + L_m) \end{bmatrix} \begin{bmatrix} I_{F1} \\ I_{F2} \end{bmatrix} \quad (59)$$

When Equation (59) is transformed relative to  $I_{F1}$ , the following equation is obtained:

$$I_{F1} = \frac{(p + j\omega_1)L_m}{R_1 + (p + j\omega_1)(L_1 + L_m)} I_{F2} + V_{F1} \quad (60)$$

In this analysis, stator voltage is the fundamental voltage source, then,  $V_{F1} = 0$  is defined. When  $I_{F1}$  is expressed by  $I_{d2}$  and  $I_{q2}$ , using Equation (60) and  $I_{F2} = (1/\sqrt{2})(I_{d2} + jI_{q2})$ , the following expression is derived:

$$I_{F1} = \frac{(p + j\omega_1)L_m}{R_1 + (p + j\omega_1)(L_1 + L_m)} \frac{1}{\sqrt{2}} (I_{d2} + jI_{q2}) \quad (61)$$

Equation (59) is substituted into Equations (57) and (58). Applying Laplace transformation, the stator current is calculated. A-phase stator current is derived as follows:

$$I_{a1} = \sum_m \sum_n \begin{aligned} & C_{(6n-1)m} \text{Cos}\{(6m+1)\theta_1 - 6n\theta_s\} \\ & + C_{(6n-5)m} \text{Cos}\{(6m-1)\theta_1 - (6n-1)\theta_s\} \\ & + D_{(6n-1)m} \text{Cos}\{(6m-1)\theta_1 + 6n\theta_s\} \\ & + D_{(6n-5)m} \text{Cos}\{(6m+1)\theta_1 + (6n-1)\theta_s\} \end{aligned} \quad (62)$$

where

$$C_{(6n-1)m} \approx A_{(6n-1)m} \left( \frac{L_m}{(L_m + L_1)} \right), D_{(6n-1)m} \approx B_{(6n-1)m} \left( \frac{L_m}{(L_m + L_1)} \right)$$

$$C_{(6n-5)m} \approx A_{(6n-5)m} \left( \frac{L_m}{(L_m + L_1)} \right), D_{(6n-5)m} \approx B_{(6n-5)m} \left( \frac{L_m}{(L_m + L_1)} \right)$$

The results of this analysis show that the harmonic currents fed to the rotors winding are transmitted to the stator windings by changing its frequency. The rotor harmonic currents at  $6m\omega_1 \pm (6n-5)\omega_s$  change to stator harmonic currents at  $(6m \pm 1)\omega_1 \pm 6(n-1)\omega_s$ . And the rotor harmonic currents at  $6m\omega_1 \pm (6n-1)\omega_s$  change to stator harmonic currents at  $(6m \pm 1)\omega_1 \pm 6n\omega_s$ . This is the effect of the rotating speed of the wound rotor induction generator. Moreover, the ratio between the amplitude of harmonic currents in the rotor and the stator is nearly 1:1.

Analysis results are verified by the experimental system shown in Fig. 6. Table 2 gives an example of experimental results. It is seen that experimental values well match with the theoretical ones. Thus, experiments confirmed that the analysis gives reliable results.

| Rotor Harmonic Current |                    | Stator Harmonic Current |                    |                   |
|------------------------|--------------------|-------------------------|--------------------|-------------------|
| Frequency              | Experimental Value | Frequency               | Experimental Value | Theoretical Value |
| 296.7 Hz               | 3.18 A             | 250 Hz                  | 2.99 A             | 3.12 A            |
| 303.3 Hz               | 1.65 A             | 350 Hz                  | 1.53 A             | 1.61 A            |
| 293.3 Hz               | 0.43 A             | 340 Hz                  | 0.46 A             | 0.42 A            |
| 316.7 Hz               | 0.40 A             | 260 Hz                  | 0.36 A             | 0.39 A            |

**Table 2.** Experimental results ( $\omega_1=50$  Hz,  $\omega_s=50$  Hz,  $m=1$ ,  $N=1400$  r/min,  $I_1=I_2=25$  A) [25]

It has been proved by experiment that this control system can control the active and reactive power independently and stably. In addition, it has been confirmed by analysis and experiment that the harmonic currents fed to the rotor windings of the generator are transmitted to the stator windings changing its frequency [25].

### 3.3. Proposed experimental setup

By using the computer and driver/buffer, the experimental setups to control active and reactive power of the wound rotor induction generator independently and stably are shown in Figs. 20 and 21 [28]. The terminals in experimental setups shown in Figs. 20 and 21 are numbered considering that the three-pulse cycloconverter with a total of 18 thyristors shown in Fig. 15a will be used.

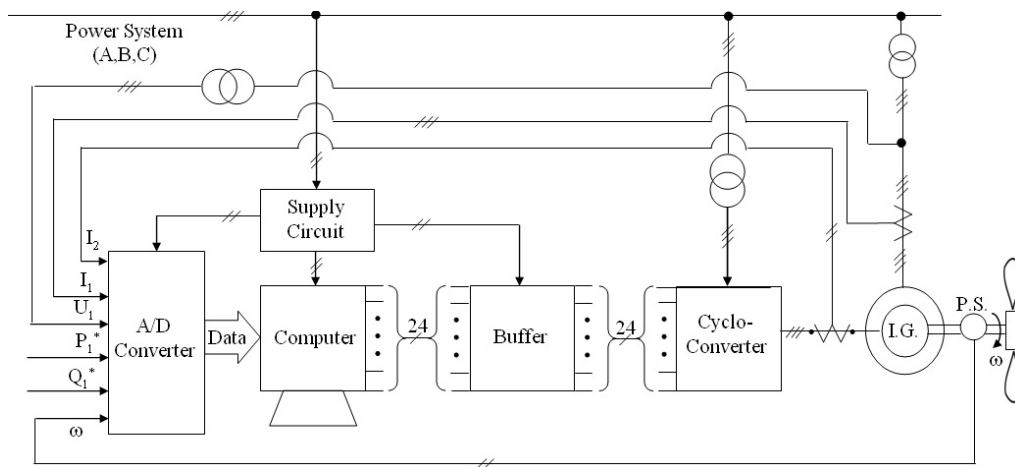


**Figure 20.** Schematic block diagram of the experimental setup for computer-aided power control of wound rotor induction generator

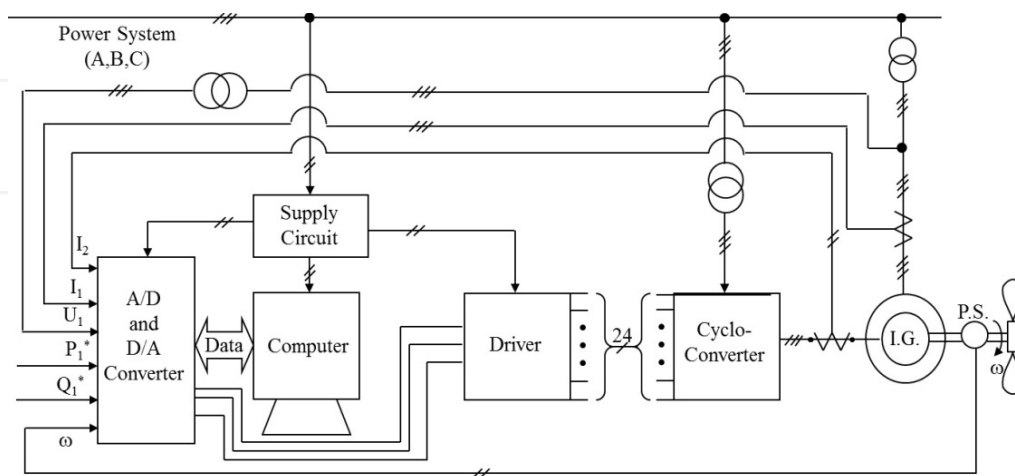


**Figure 21.** Another schematic block diagram of the experimental setup for computer-aided power control of wound rotor induction generator

## 4. Conclusion

New configurations for power control system of the doubly-fed wound rotor induction generator have been proposed. These configurations are based on a control method using a rotating reference frame fixed on the air-gap flux of the generator. By using them, the active and reactive power of generator can be controlled independently and stably. To achieve this purpose, power and current control that are fundamental subjects have been analyzed and as a result, a computer-aided circuit is given to achieve the power and current control. Using computers enables application of new technologies for easier control. For example, any new metaheuristic techniques or classification/identification techniques could be applied by just changing the code in the computer.

## Author details

Fevzi Kentli\*

Address all correspondence to: [fkentli@marmara.edu.tr](mailto:fkentli@marmara.edu.tr)

Marmara University- Faculty of Technology – Department of Mechatronics Engineering  
Kadıköy-Istanbul, Turkey

## References

- [1] Boldea I. *The Electric Generators Handbook*. Florida, USA: Taylor & Francis; 2006. p. 552.
- [2] Induction Generator [Internet]. [Updated: March 2015]. Available from: <http://www.alternative-energy-tutorials.com/wind-energy/induction-generator.html> [Accessed: March 2015]
- [3] Nidec Motor Corporation. Induction Generator [Internet]. Available from: <http://www.usmotors.com/TechDocs/ProFacts/Induction-Generator.aspx> [Accessed: March 2015]
- [4] Liserre M, Cárdenas R, Molinas M, Rodríguez J. Overview of multi-MW wind turbines and wind parks. *IEEE Transact Indus Electron*. 2011;58(4):1081-1095. DOI: 10.1109/TIE.2010.2103910
- [5] Datta R, Ranganathan V T. Direct power control of grid-connected wound rotor induction machine without rotor position sensors. *IEEE Transact Power Electron*. 2001;16(3):390-399. DOI: 10.1109/63.923772

- [6] Nakra H L, Dube B. Slip power recovery induction generators for large vertical axis wind turbines. *IEEE Transact Energy Convers.* 1988;3(4):733-737. DOI: 10.1109/60.9346
- [7] Herrera J I, Reddoch T W, Lawler J S. Harmonics generated by two variable speed wind generating systems. *IEEE Transact Energy Convers.* 1988;3(2):267-273. DOI: 10.1109/60.4729
- [8] Holmes P G, Elsonbaty N A. Cycloconverter-excited divided-winding doubly-fed machine as a wind-power converter. *IEE Proc B.* 1984;131(2):61-69. DOI: 10.1049/ip-b.1984.0010
- [9] Akagi H, Sato H. Control and performance of a doubly-fed induction machine intended for a flywheel energy storage system. *IEEE Transact Power Electron.* 2002;17(1):109-116. DOI: 10.1109/63.988676
- [10] Betz R E, Cook B J. Instantaneous power control of induction machines. *J Electric Electron Engin.* 2001;21(1):57-63.
- [11] Lei S, Zengqiang M, Yang Y, Tao W, Haifeng T. Active power and reactive power regulation capacity study of DFIG wind turbine. In: International Conference on Sustainable Power Generation and Supply; 6-7 April 2009; Nanjing, China. IEEE; 2009. p. 1-6. DOI: 10.1109/SUPERGEN.2009.5348144
- [12] Jiabing H, Heng N, Bin H, Yikang H, Zhu Z Q. Direct active and reactive power regulation of DFIG using sliding-mode control approach. *IEEE Transact Energy Convers.* 2010;25(4):1028-1039. DOI: 10.1109/TEC.2010.2048754
- [13] Verij K M, Moradi M, Verij K R. Minimization of powers ripple of direct power controlled DFIG by fuzzy controller and improved discrete space vector modulation. *Electric Power Sys Res.* 2012;89:23-30. DOI: 10.1016/j.epsr.2012.02.008
- [14] Arnalte S, Burgos J C, Rodriguez-Amenedo J L. Direct torque control of a doubly-fed induction generator for variable speed wind turbines. *Electric Power Comp Sys.* 2002;30(2):199-216. DOI: 10.1080/153250002753427851
- [15] Huang H, Fan Y, Qiu R C, Jiang X D. Quasi-steady-state rotor EMF oriented vector control of doubly fed winding induction generators for wind-energy generation. *Electric Power Comp Sys.* 2006;34(11):1201-1211. DOI: 10.1080/15325000600698597
- [16] Sang C L, Kwang H N. Dynamic modelling and passivity-based control of an induction motor powered by doubly fed induction generator. In: Industry Applications Conference: 38th IAS Annual Meeting; 12-16 October 2003; Utah, USA. New Jersey, USA: IEEE; 2003. p. 1970-1975. DOI: 10.1109/IAS.2003.1257837
- [17] Muljadi E, Butterfield C P. Pitch-controlled variable-speed wind turbine generation. *IEEE Transact Indust Applic.* 2001;37(1):240-246. DOI: 10.1109/28.903156

- [18] Fadaeinedjad R, Moallem M, Moschopoulos G. Simulation of a wind turbine with doubly fed induction generator by fast and simulink. *IEEE Transact Energy Convers.* 2008;23(2):690-700. DOI: 10.1109/TEC.2007.914307
- [19] Zin A A B M, Pesaran H A M, Khairuddin A B, Jahanshaloo L, Shariati O. An overview on doubly fed induction generators' controls and contributions to wind based electricity generation. *Renew Sustain Energy Rev.* 2013;27:692-708. DOI: doi:10.1016/j.rser.2013.07.010
- [20] Xu L, Cheng W. Torque and reactive power control of a doubly fed induction machine by position sensorless scheme. *IEEE Transact Indust Applic.* 1995;31(3):636 - 642. DOI: 10.1109/28.382126
- [21] Datta R, Ranganathan V T. Decoupled control of active and reactive power for a grid-connected doubly-fed wound rotor induction machine without rotor position sensors. In: *IEEE Industry Applications Conference: Thirty-Fourth Ias Annual Meeting*; 3-7 October 1999; Arizona, USA. IEEE; 1999. p. 2623-2630.
- [22] Morel L, Godfroid H, Mirzaian A, Kauffmann J M. Double-fed induction machine: Converter optimisation and field oriented control without position sensor. *IEE Proc B.* 1998;145(4):360-368. DOI: 10.1049/ip-epa:19981982
- [23] Bogalecka E. Power control of a double fed induction generator without speed or position sensor. In: *Fifth European Conference on Power Electronics and Applications*; 13-16 September 1993; Brighton, England. London, England: Institution of Electrical Engineers; 1993. p. 224-228.
- [24] Leonhard W. *Control of Electrical Drives*. 1st edn. New York, USA: Springer-Verlag; 1985. p. 346.
- [25] Yamamoto M, Motoyoshi O. Active and reactive power control for doubly-fed wound rotor induction generator. *IEEE Transact Power Electron.* 1991;6(4):624-629. DOI: 10.1109/63.97761
- [26] Brune C, Spee R, Wallace A K. Experimental evaluation of a variable-speed, doubly-fed wind-power generation system. In: *IEEE Industry Applications Conference: 28th IAS annual meeting*; 2-8 October 1993; Ontario, Canada. New Jersey, USA: Institute of Electrical & Electronics Engineers; 1993. p. 480-487.
- [27] Bhowmik S, Spee R, Enslin J H L. Performance optimization for doubly-fed wind power generation systems. In: Cramer, Don et al. (eds.). *Industry Applications Conference, The 1998 IEEE Conference*; 12-15 October 1998; Missouri, USA. New York, USA: The Institute of Electrical and Electronic Engineers, Inc; 1998. p. 2387-2394.
- [28] Kentli F. Computer aided power control for wound rotor induction generator. *Ozean J Appl Sci.* 2009;2(1):39-48.

- [29] Akagi H, Kanazawa Y, Nabae A. Instantaneous reactive power compensators comprising switching devices without energy storage components. *IEEE Transact Indust Applic.* 1984;20(3):625-630. DOI: 10.1109/TIA.1984.4504460
- [30] Cyril W. Lander. *Power Electronics*. 3rd ed. England: McGraw-Hill Publishing Company; 1993. p. 480.
- [31] Erwin Kreyszig. *Advanced Engineering Mathematics*. 3rd edn. New York: Wiley; 1972. p. 866.
- [32] Pelly B R. *Thyristor Phase-Controlled Converter and Cycloconverters*. 1st edn. Wiley-Blackwell; 1971. p. 434.

IntechOpen

